

Scattering of two and three physical pions at maximal isospin from lattice QCD

Matthias Fischer,^{1,2} Bartosz Kostrzewa,³ Liuming Liu,⁴ Fernando Romero-López,⁵ Martin Ueding,^{1,2} and Carsten Urbach^{1,2}

(Extended Twisted Mass Collaboration)

¹*Helmholtz-Institut für Strahlen- und Kernphysik, University of Bonn, 53115 Bonn, Germany*

²*Bethe Center for Theoretical Physics, University of Bonn, 53115 Bonn, Germany*

³*High Performance Computing and Analytics Lab, University of Bonn, 53115 Bonn, Germany*

⁴*Institute of Modern Physics, Chinese Academy of Sciences, Lanzhou 730000, China*

⁵*Instituto de Física Corpuscular, Universitat de València and CSIC, 46980 Paterna, Spain*

(Dated: August 10, 2020)

We present the first direct $N_f = 2$ lattice QCD computation of two- and three- π^+ scattering quantities that includes an ensemble at the physical point. We study the quark mass dependence of the two-pion phase shift, and the three-particle interaction parameters. We also compare to phenomenology and chiral perturbation theory (ChPT). In the two-particle sector, we observe good agreement to the phenomenological fits in s - and d -wave, and obtain $M_\pi a_0 = 0.0481(86)$ at the physical point from a direct computation. In the three-particle sector, we observe reasonable agreement at threshold to the leading order chiral expansion, i.e. a mildly attractive three-particle contact term. In contrast, we observe that the energy-dependent part of the three-particle quasiloocal scattering quantity is not well described by leading order ChPT.

Introduction.— In physics, two-body problems are analytically solvable for many interaction potentials, e.g. the famous Kepler problem. This is no longer the case for three-body—not to mention n -body—problems, for which one typically needs to resort to numerical solutions. Maybe that is one of the reasons why quantum field theories can in general only be solved approximately by expanding around the non-interacting case: all possible n -body interactions need to be taken into account. In quantum chromodynamics (QCD), the theory of strong interactions, even such a perturbative approach fails at low energies due to the non-existence of a small expansion parameter: the theory is strongly coupled.

QCD describes the interaction of quarks and gluons, while only hadrons (mesons and baryons) are experimentally observable. They are low energy bound states, or resonances of the former fundamental particles. Understanding the interaction of two or more hadrons is highly relevant for several reasons. For instance, resonances become visible only when studying the interaction of other hadrons. And for understanding experimental signatures of particle decays, the interactions of the final states need to be understood.

The formulation of QCD on a spacetime lattice—lattice QCD—offers the opportunity of first principles, numerical explorations of low-energy hadronic observables. Among those are few-particle scattering amplitudes, especially those which are difficult to access experimentally. Examples of these are near-threshold two-particle scattering, and matrix elements involving three particles in the final and/or initial state. Maybe the most obvious example for the importance of three particle interactions is the ω -meson, which decays predominantly into three

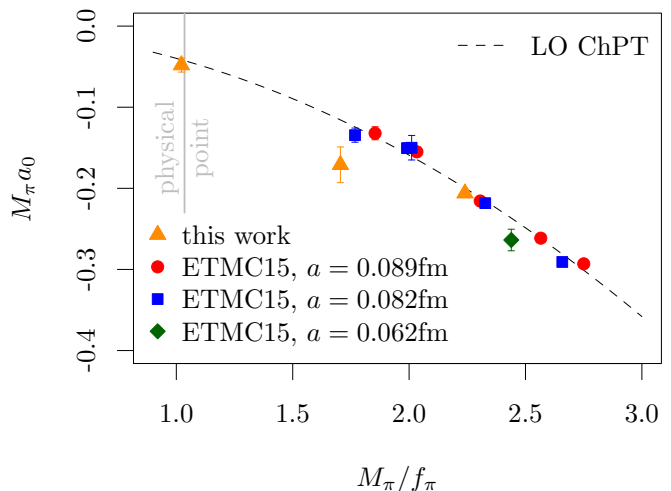


FIG. 1. $I = 2$ scattering length $M_\pi a_0$ as a function of M_π/f_π comparing the $N_f = 2 + 1 + 1$ ETMC twisted mass results [3] with this work. The dashed line represents the leading order ChPT prediction.

pions in a p -wave [1]. Another one would be the Roper resonance [2], with both $N\pi$ and $N\pi\pi$ decay channels. However, since the investigation of three particle interactions from lattice QCD is in its infancy, three weakly interacting pions with isospin $I = 3$ represent an interesting and important benchmark system.

The extraction of two-particle scattering amplitudes in Lattice QCD is by now well established for $2 \rightarrow 2$ systems, both theoretically [4–16], and in practice [3, 17–38] (see Ref. [39] for a review). One of the most studied systems is isospin-2 $\pi\pi$ scattering. To illustrate the state-of-the-art, we show in Figure 1 the $\pi\pi$ $I = 2$ scat-

tering length $M_\pi a_0$ as a function of M_π/f_π comparing this work's result to the $N_f = 2 + 1 + 1$ results of Ref. [3]. The new $N_f = 2$ point at the physical value of M_π/f_π is compatible within errors with leading order (LO) ChPT (dashed line).

Over the last few years, theoretical and numerical work investigating three-particle scattering amplitudes from lattice QCD emerged as a hot topic. The finite-volume formalism exists following three different approaches: (i) generic relativistic effective field theory (RFT) [40–49], (ii) nonrelativistic effective field theory (NREFT) [50–55], and (iii) (relativistic) finite volume unitarity (FVU) [56, 57] (see also Refs. [58–60] and Ref. [61] for a review). Lattice data [62–64] has been confronted to both, the FVU [57, 63, 64] and RFT [65] formalism. A related approach used in the literature consists of using the ground state and the threshold expansion, which is valid only for weakly interacting systems [66–69].

In this letter, we present results for scattering quantities of two and three-pion with maximal isospin, including for the first time an ensemble at the physical point. This work breaks new ground on several fronts: the first direct computation at the physical point of the $I = 2$ s -wave phase shift and d -wave scattering amplitude, and the chiral dependence of the three- π^+ quasilocal interaction.

Scattering amplitudes from lattice QCD—Due to the lack of asymptotic states in finite volume, the calculation of scattering amplitudes from lattice simulations proceeds in an indirect way. The required physical quantities from the lattice are the finite-volume interacting energies of two and three particles—the spectrum. The mapping between the finite volume spectrum and infinite-volume scattering quantities—the so-called quantization condition—is known but highly nontrivial (valid up to exponentially-suppressed corrections on $M_\pi L$).

The two-particle quantization condition (QC2) takes the form of a determinant equation [4–6] (for simplicity we assume here two identical scalars):

$$\det [F_2^{-1}(\mathbf{P}, E^*, L) + \mathcal{K}_2(E^*)] = 0. \quad (1)$$

Here, F_2 and \mathcal{K}_2 are both matrices in angular momentum space ℓ, m . On the one hand, the matrix elements of F_2 are kinematical functions (Lüscher zeta function) that depend on the three-momentum of the system, \mathbf{P} and the center-of-mass (CM) energy, E^* . On the other hand, $(\mathcal{K}_2)_{\ell m, \ell' m'} = \delta_{\ell m, \ell' m'} (\mathcal{K}_2)_\ell$ is simply the infinite-volume scattering K-matrix projected to the corresponding partial wave. In order to render the matrices finite-dimensional, a truncation must be applied in ℓ, ℓ' by assuming that \mathcal{K}_2 vanishes for higher partial waves. Typically, only the lowest one or two waves are kept. Furthermore, the relations between \mathcal{K}_2 , the phase shift (δ_ℓ), and the physical scattering amplitude (\mathcal{M}_2) are trivial. More details can be found in Ref. [39].

The three-particle quantization condition (QC3) for identical (pseudo)scalars in the RFT approach reads (G-parity is assumed) [40]:

$$\det [F_3^{-1}(E, \mathbf{P}, L) + \mathcal{K}_{3,\text{df}}(E^*)] = 0. \quad (2)$$

Even though this looks formally identical to Eq. 1, there are some distinct features. First, the matrices in Eq. 2 live in a larger $k \ell m$ space, where ℓ, m are the angular momentum indices of the interacting pair, and k labels the three-momentum of the third particle—the spectator. Next, F_3 depends on geometric functions (like F_2 itself), but also on \mathcal{K}_2 . Thus, two-particle interactions are a *necessary* ingredient for three-particle scattering. Finally, $\mathcal{K}_{3,\text{df}}$ is a real, singularity-free, quasiloal, intermediate three-particle scattering quantity—which we aim to determine. As in the case of the QC2, Eq. 2 is infinite-dimensional, and must be truncated. The truncation in k is due to a cut-off function, whereas for ℓ, m one assumes that $\mathcal{K}_{3,\text{df}}$ vanishes above some value of ℓ , see Refs. [40, 61] for details. Establishing the connection between $\mathcal{K}_{3,\text{df}}$ and the physical scattering amplitude, \mathcal{M}_3 requires a set of integral equations, which were derived in Ref. [41]. These equations have been solved only below and at the three-particle threshold [45]. In this work, we focus only on the extraction of $\mathcal{K}_{3,\text{df}}$ and leave the relation $\mathcal{K}_{3,\text{df}} \leftrightarrow \mathcal{M}_3$ for future work.

In a finite volume, partial waves mix and, thus, F_2 and F_3 in Eqs. 1 and 2 are non diagonal in ℓ, m . Therefore, in a finite volume the correct labels are irreducible representations (irreps) of the discrete symmetry group, which we label as Γ . The subduction of angular momenta into irreps is well known [70, Table 2]. Therefore, one block-diagonalizes the quantization conditions into irreps, see Refs. [16, 47, 54, 65].

Ensemble	$L^3 \times T$	M_π/MeV	aM_π	M_π/f_π	# confs.
cA2.60.32	$32^3 \times 64$	340	0.1578(1)	2.235(6)	337
cA2.30.48	$48^3 \times 96$	242	0.11195(7)	1.705(3)	350
cA2.09.48	$48^3 \times 96$	134	0.06205(4)	1.022(1)	1604

TABLE I. $N_f = 2$ Ensembles used in this work. The lattice spacing is $a = 0.0914(15)$ fm, and $c_{\text{SW}} = 1.57551$. For the decay constant we use the normalization $f_\pi = \sqrt{2}F_\pi$. M_π/f_π has been corrected for finite size effects according to Refs. [71–73].

Lattice computation.— This work uses $N_f = 2$ flavour lattice QCD ensembles generated by the Extended Twisted Mass collaboration (ETMC) [74], including one ensemble at the physical pion mass—see Table I¹. For the ensemble

¹ The ensemble cA2.30.48 has largest statistical uncertainties for the scattering parameters. There are two reasons for this: first, the number of configuration is much lower than in the cA2.09.48 ensemble; second, the energy shift of the interacting energies with respect to the free energies is less significant than in the cA2.60.32 ensemble.

ble generation the Iwasaki gauge action [75] was used together with Wilson clover twisted mass fermions at maximal twist [76]. The latter guarantees scaling towards the continuum with only $O(a^2)$ artefacts in the lattice spacing a [77]. The presence of the clover term (with coefficient c_{sw}) has been shown to further reduce the $O(a^2)$ artefacts, in particular isospin breaking effects of the twisted-mass formulation which have been empirically found to be very small for masses and decay constants [74]. For the two pion scattering length with isospin $I = 2$, discretisation artefacts have been shown to be only of order $O(am_q)^2$, with m_q the up/down quark mass [78]. Parametrically, $O(a^2)$ artefacts are of order 2.5% and $O(am_q)^2$ even $\leq 0.4\%$ for the lattice spacing value used here, and thus well below the statistical uncertainty we obtain.

The two- and three- π^+ energy spectrum is measured from Euclidean correlation functions of operators with the corresponding quantum numbers. By means of the single pion operators ($\pi^+ = -\bar{u}\gamma_5 d$), we construct two-particle operators as follows:

$$O_{\pi\pi}(p_1, p_2) = \sum_{x,y} e^{ip_1x+ip_2y} \pi^+(x) \pi^+(y), \quad (3)$$

where p_i labels the momentum of each single pion, and similarly for three pions. Correlation functions are computed using the stochastic Laplacian-Heaviside smearing [79, 80] with algorithmic parameters identical to the ones chosen in Ref. [81]. In addition, operators that transform under a specific irrep of a discrete symmetry group are constructed by projecting as in Ref. [32]. We then extract the spectrum in each irrep independently using the generalized eigenvalue method (GEVM) [6, 82, 83] and also the GEVM/PGEVM method [84], see Ref. [85] for more details.

A technical issue that affects lattice calculations with (anti)periodic boundary conditions in the time direction is the presence of so-called thermal states, i.e. effects from pions that propagate backwards in time across the boundary. They vanish with $M_\pi T \rightarrow \infty$, but may be significant for some energy levels for smaller $M_\pi T$ -values. Different techniques are employed to handle them: one can either remove them using weighting and shifting [70], explicitly fit them, or attempt to fit early enough in Euclidean time. An alternative approach is to fit ratios of correlators [17]. Here, we use various of these methods with manually chosen fit ranges [85]. Then, we perform a correlated and weighted average over the different methods. The differences are interpreted as a systematic error and incorporated into the statistical error by widening the resampling distribution [32, 85]. The energy levels are publicly available [86].

Results.— By keeping only the leading partial wave in irrep A_{1g} (A_1) in $\mathbf{P} = 0$ ($\mathbf{P} \neq 0$), the projected QC2 becomes a one-to-one correspondence of an energy level

to a s -wave phase shift point [6, 7]. For the analysis, we need an appropriate phase shift parametrization. We use a model that incorporates the expected Adler zero [65, 89]:

$$\frac{k}{M_\pi} \cot \delta_0 = \frac{\sqrt{s}}{M_\pi(s - 2z^2)} \left(B_0 + B_1 \frac{k^2}{M_\pi^2} + \dots \right). \quad (4)$$

We will fix the position of the Adler zero to its leading order Chiral Perturbation Theory (LO ChPT) value: $z^2 = M_\pi^2$. Even though higher order corrections are to be expected, its value has been seen to be compatible to LO ChPT when left free [87, 90, 91]. Note that in Eq. 4 with fixed Adler zero, the scattering length is given by $M_\pi a_0 = -1/B_0$.

	$1/B_0$	B_1	B_2	χ^2/dof
cA2.60.32	-0.2090(54)	-2.3(3)	—	19.06/(16-2)
cA2.60.32	-0.2110(57)	-3.1(6)	0.4(2)	15.96/(16-3)
cA2.30.48	-0.160(23)	-1.8(6)	—	15.30/(16-2)
cA2.09.48	-0.0477(90)	-1.4(1.2)	—	11.08/(10-2)

TABLE II. s -wave fit results for the various ensembles using Eq. 4 with fixed $z_2^2 = M_\pi^2$. Here we use only the two-pion levels in the A_{1g} and A_1 irreps.

We perform a correlated two-parameter fit to the energy levels. The results for the three ensembles are shown in Table II. In all cases, the magnitude of the B_i coefficients decreases with increasing order, indicating that the expansion converges quickly enough even at the heaviest pion mass. Still, for the heaviest ensemble (cA2.60.32), we also attempt a fit with a quadratic term in k^2 , B_2 and observe a small, barely significant value for B_2 and no substantial change in B_0 and B_1 . Based on ChPT, better convergence is expected for lighter pions.

Similarly, the d -wave phase shift can be obtained from most of the non-trivial irreps when neglecting $\ell > 2$ waves [15, 16]. Since we have few data points only, we attempt the following fit:

$$\frac{k^5}{M_\pi^5} \cot \delta_2 = -\frac{1}{M_\pi^5 a_2}. \quad (5)$$

We show our fit results in Table III, with the included values of E^* .

Next, we parametrize $\mathcal{K}_{3,\text{df}}$. For this, we expand $\mathcal{K}_{3,\text{df}}$ about threshold up to linear terms of relativistic invariants [47]: For the extraction of the three-body scattering quantity,

$$\mathcal{K}_{3,\text{df}} = \mathcal{K}_{\text{df},3}^{\text{iso},0} + \mathcal{K}_{\text{df},3}^{\text{iso},1} \Delta, \quad \Delta = \frac{(E^*)^2 - 9M_\pi^2}{9M_\pi^2}, \quad (6)$$

where $\mathcal{K}_{\text{df},3}^{\text{iso},0}$ and $\mathcal{K}_{\text{df},3}^{\text{iso},1}$ are the numerical constants to be determined. This parametrization has no momentum dependence, and thus receives the name ‘‘isotropic’’. It is the three-particle equivalent of keeping only s -wave

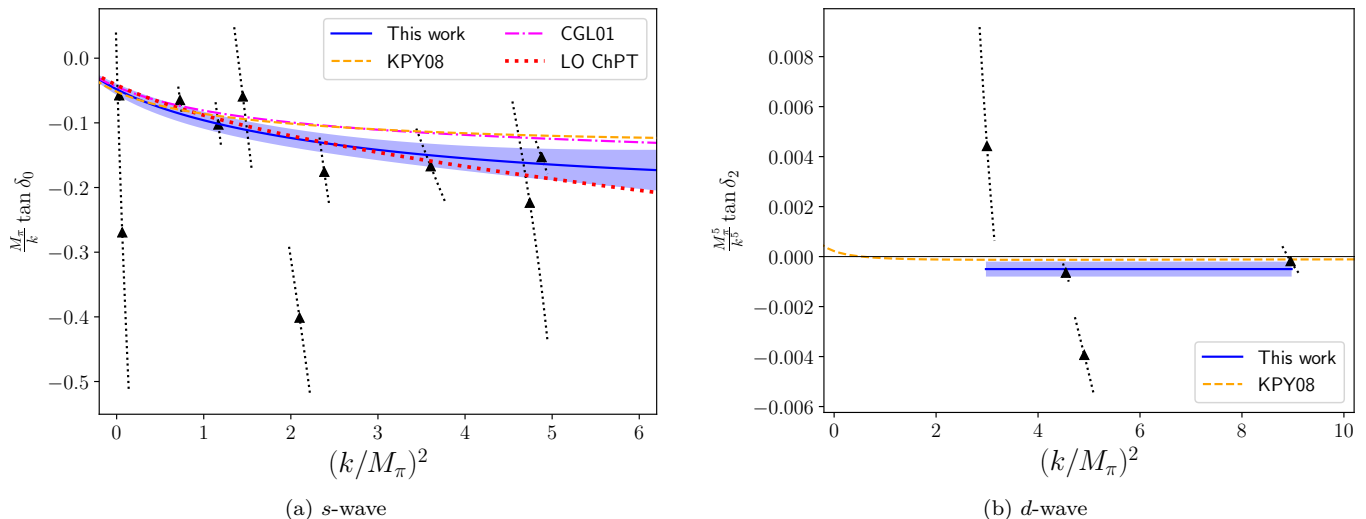


FIG. 2. s - and d -wave phase shift at the physical point (ensemble cA2.09.48) compared to the fits to experimental data (KPY08) in [87] and (CGL01) in [88]. For s -wave we use a model that incorporates the Adler-zero, whereas for d -wave we fit to a constant in the region for which we have data.

interactions. Momentum dependence enters at $O(\Delta^2)$ in the parametrization, for which also the d -wave must be included [47].

Following the strategy outlined in Ref. [65], we perform a simultaneous s -wave only fit to two- π^+ A_1 levels, and all three- π^+ levels. For this, we use the δ_0 model in Eq. 4 with B_0 , B_1 and fixed $z_2^2 = M_\pi^2$; and the $\mathcal{K}_{3,\text{df}}$ parametrization in Eq. 6—four parameters in total. We show the fit results for all three ensembles in Table IV. As can be seen the best fit values for B_0 and B_1 agree well between the two-particle and the global fit, with even smaller errors in the case of the latter.

	$M_\pi^5 a_2$	χ^2/dof	CM energy range
cA2.60.32	0.0037(8)	15.03/(12-1)	$[3.2M_\pi, 4.4M_\pi]$
cA2.30.48	0.007(2)	16.89/(10-1)	$[2.8M_\pi, 4.2M_\pi]$
cA2.09.48	0.0005(3)	7.33/(4-1)	$[4.0M_\pi, 6.3M_\pi]$

TABLE III. d -wave two-pion fits to Eq. 5. Here we use only non- A_1 two-pion levels. The last column shows the energy range for which data is used.

Discussion.— Starting with δ_0 , we show in Figure 2a all phase shift data points, and include the best fit curve from the two- and three- π^+ global fit. As can be seen, the difference to LO ChPT is small, and due to the fit parameter $B_1 \neq 0$. In addition, our results agree within $< 2\sigma$ with the fits in Refs. [87, 88]. For the scattering length, we obtain $M_\pi a_0 = 0.0481(86)$ (see Table IV), which also agrees well with all phenomenological determinations [87, 88, 90–92], and other lattice results obtained indirectly by extrapolating to the physical point using ChPT [3, 17, 34, 93–99], see Figure 1.

Regarding the d -wave phase shift, we have mild statistical

evidence that at the physical point it is repulsive in the considered energy region. We observe agreement within $\gtrsim 1\sigma$ with Ref. [87], as shown in Figure 2b. An interesting feature of the phenomenological fits to δ_2 is that there is a sign change near threshold, which yields an attractive phase shift at threshold—negative a_2 in our convention [87, 90, 91, 100]. We cannot confirm or deny such behaviour, as the explored energy region is too far above threshold. For larger pion mass values, we obtain similar behaviour, with increasingly repulsive d -wave phase shift as the mass grows—see Table III and Ref. [85].

We show our results in the three-particle sector in Figure 3. As can be seen in Figure 3a, there is significant evidence that $\mathcal{K}_{3,\text{df}}$ at threshold ($\mathcal{K}_{\text{df},3}^{\text{iso},0}$) is positive (attractive). Even though we find reasonable agreement with the LO ChPT [65] prediction, our data combined with Ref. [65] suggests that its magnitude may be larger than the one predicted by LO ChPT. Thus, NLO effects can be significant, and it may be worth to extend the ChPT result to one loop. For $\mathcal{K}_{\text{df},3}^{\text{iso},1}$, the situation is somewhat different. All evidence points to a negative value, very far from the ChPT results. There are few possibilities to explain this. Besides the obvious NLO ChPT explanation, there is a subtlety in the LO ChPT prediction. It uses the fact that the connection between $\mathcal{K}_{3,\text{df}}$ and the physical three-pion scattering amplitude—which involves integral equations—is trivial to leading order in ChPT [65]:

$$\mathcal{K}_{3,\text{df}} = \mathcal{M}_{3,\text{df}} [1 + O(M_\pi^2/F_\pi^2)], \quad (7)$$

where $\mathcal{M}_{3,\text{df}}$ is the divergence-free three-to-three amplitude [41]. As argued in Ref. [65], this induces large errors in $\mathcal{K}_{\text{df},3}^{\text{iso},1}$ (up to 50% for 200 MeV pions). The situation

	$1/B_0$	B_1	$M_\pi^2 \mathcal{K}_{df,3}^{iso,0}$	$M_\pi^2 \mathcal{K}_{df,3}^{iso,1}$	χ^2/dof
cA2.60.32	-0.2061(49)	-1.9(2)	4500(1500)	-6200(1800)	58.89/(43-4)
cA2.30.48	-0.171(22)	-2.0(5)	7500(5600)	-13000(5000)	36.30/(33-4)
cA2.09.48	-0.0481(86)	-1.3(1.1)	0(800)	-200(500)	19.06/(19-4)

TABLE IV. Two- and three-pion fits using the Adler-zero form ($z^2 = M_\pi^2$, fixed). Since we only include s -wave interactions, we use two-pion levels in the A_1 irrep, and all irreps for three-pions.

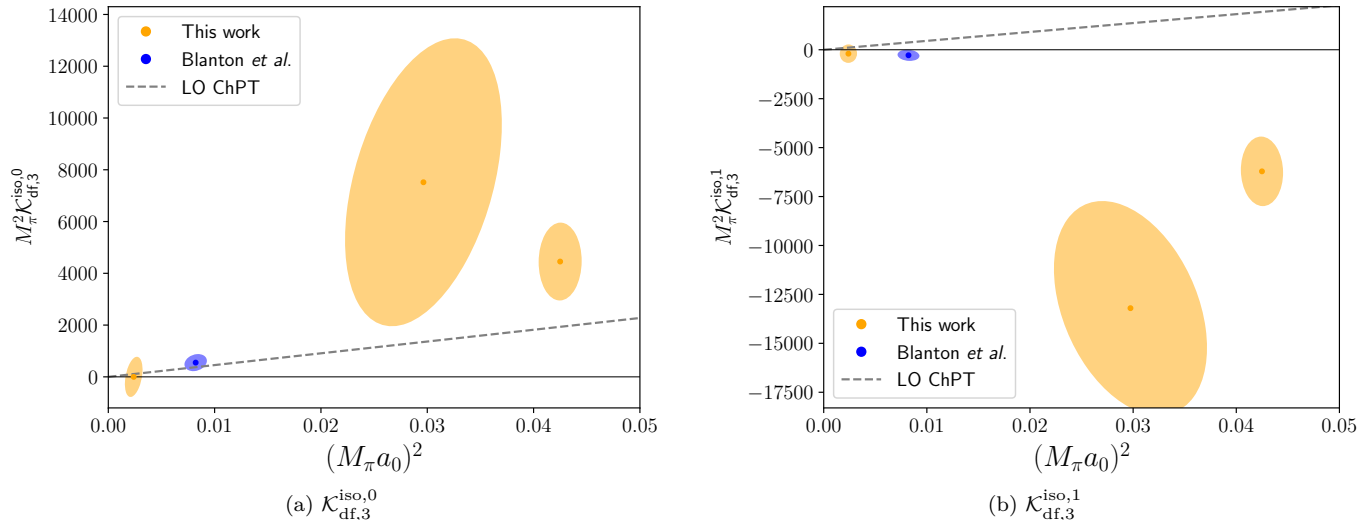


FIG. 3. Constant(left) and linear(right) terms of $\mathcal{K}_{3,df}$ as a function of the s -wave scattering length. We also include the results of Ref. [65].

is expected to be more dramatic for heavier pions, like our two results at 242 and 340 MeV, for which the largest difference is seen. In order to address this rigorously, the integral equation must be systematically solved, which is beyond the scope of this work.

Conclusion.—We have presented the first $N_f = 2$ lattice calculation of two- and three- π^+ scattering at the physical point. Our results show reasonable agreement with other lattice calculations that extrapolate to the physical point, with phenomenological fits, and also with ChPT. By including two ensembles at heavier pion masses, we have been able to gain insight on the chiral dependence of two- and three- π^+ scattering quantities.

This letter represents a step towards exploring and understanding the hadronic spectrum of QCD, and shows that three-particle quantities are feasible with current technology. In the very near future we expect more lattice calculations of three-body observables with increasing accuracy and describing systems with growing complexity—e.g. three-particle resonances such as the ω .

Acknowledgements.— We thank all members of ETMC for the most enjoyable collaboration. We also thank P. Hernández, A. Rusetsky, and S. Sharpe for comments on the manuscript. The authors gratefully acknowledge the Gauss Centre for Supercomputing e.V. (www.gauss-centre.eu) for funding this project

by providing computing time on the GCS Supercomputer JUQUEEN [101] and the John von Neumann Institute for Computing (NIC) for computing time provided on the supercomputers JURECA [102] and JUWELS [103] at Jülich Supercomputing Centre (JSC). This project was funded in part by the DFG as a project in the Sino-German CRC110. FRL acknowledges the support provided by the European projects H2020-MSCA-ITN-2015/674896-ELUSIVES, H2020-MSCA-RISE-2015/690575-InvisiblesPlus, the Spanish project FPA2017-85985-P, and the Generalitat Valenciana grant PROMETEO/2019/083. The work of FRL also received funding from the European Union Horizon 2020 research and innovation program under the Marie Skłodowska-Curie grant agreement No. 713673 and “La Caixa” Foundation (ID 100010434, LCF/BQ/IN17/11620044). The open source software packages tmLQCD [104–106], Lemon [107], QUDA [108–110], R [111], hadron [112] and paramvalf [113] have been used.

-
- [1] M. Tanabashi *et al.* (PDG), “Review of particle physics,” *Phys. Rev. D* **98**, 030001 (2018).
[2] L. David Roper, “Evidence for a P_{11} pion-nucleon res-

- onance at 556 MeV,” *Phys. Rev. Lett.* **12**, 340–342 (1964).
- [3] C. Helmes, C. Jost, B. Knippschild, C. Liu, J. Liu, L. Liu, C. Urbach, M. Ueding, Z. Wang, and M. Werner (ETM), “Hadron-hadron interactions from $N_f = 2 + 1 + 1$ lattice QCD: isospin-2 $\pi\pi$ scattering length,” *JHEP* **09**, 109 (2015), arXiv:1506.00408 [hep-lat].
- [4] M. Lüscher, “Volume Dependence of the Energy Spectrum in Massive Quantum Field Theories. 2. Scattering States,” *Commun. Math. Phys.* **105**, 153–188 (1986).
- [5] Martin Lüscher, “Two particle states on a torus and their relation to the scattering matrix,” *Nucl. Phys.* **B354**, 531–578 (1991).
- [6] Martin Lüscher and Ulli Wolff, “How to Calculate the Elastic Scattering Matrix in Two-dimensional Quantum Field Theories by Numerical Simulation,” *Nucl. Phys.* **B339**, 222–252 (1990).
- [7] K. Rummukainen and Steven A. Gottlieb, “Resonance scattering phase shifts on a nonrest frame lattice,” *Nucl.Phys.* **B450**, 397–436 (1995), arXiv:hep-lat/9503028.
- [8] C. h. Kim, C. T. Sachrajda, and Stephen R. Sharpe, “Finite-volume effects for two-hadron states in moving frames,” *Nucl. Phys.* **B727**, 218–243 (2005), arXiv:hep-lat/0507006 [hep-lat].
- [9] Song He, Xu Feng, and Chuan Liu, “Two particle states and the S-matrix elements in multi-channel scattering,” *JHEP* **07**, 011 (2005), arXiv:hep-lat/0504019 [hep-lat].
- [10] V. Bernard, M. Lage, U.-G. Meißner, and A. Rusetsky, *JHEP* **1101**, 019 (2011), arXiv:1010.6018 [hep-lat].
- [11] Maxwell T. Hansen and Stephen R. Sharpe, “Multiple-channel generalization of Lellouch-Lüscher formula,” *Phys.Rev.* **D86**, 016007 (2012), arXiv:1204.0826 [hep-lat].
- [12] Raul A. Briceño and Zohreh Davoudi, “Moving multi-channel systems in a finite volume with application to proton-proton fusion,” *Phys. Rev.* **D88**, 094507 (2013), arXiv:1204.1110 [hep-lat].
- [13] Raul A. Briceño, “Two-particle multichannel systems in a finite volume with arbitrary spin,” *Phys. Rev.* **D89**, 074507 (2014), arXiv:1401.3312 [hep-lat].
- [14] F. Romero-López, A. Rusetsky, and C. Urbach, “Vector particle scattering on the lattice,” *Phys. Rev.* **D98**, 014503 (2018), arXiv:1802.03458 [hep-lat].
- [15] Thomas Luu and Martin J. Savage, “Extracting Scattering Phase-Shifts in Higher Partial-Waves from Lattice QCD Calculations,” *Phys. Rev.* **D83**, 114508 (2011), arXiv:1101.3347 [hep-lat].
- [16] M. Göckeler, R. Horsley, M. Lage, U. G. Meißner, P. E. L. Rakow, A. Rusetsky, G. Schierholz, and J. M. Zanotti, “Scattering phases for meson and baryon resonances on general moving-frame lattices,” *Phys. Rev.* **D86**, 094513 (2012), arXiv:1206.4141 [hep-lat].
- [17] Xu Feng, Karl Jansen, and Dru B. Renner, “The $\pi^+ \pi^+$ scattering length from maximally twisted mass lattice QCD,” *Phys. Lett.* **B684**, 268–274 (2010), arXiv:0909.3255 [hep-lat].
- [18] Michael Lage, Ulf-G. Meißner, and Akaki Rusetsky, “A Method to measure the antikaon-nucleon scattering length in lattice QCD,” *Phys. Lett.* **B681**, 439–443 (2009), arXiv:0905.0069 [hep-lat].
- [19] David J. Wilson, Raul A. Briceño, Jozef J. Dudek, Robert G. Edwards, and Christopher E. Thomas, “Coupled $\pi\pi, K\bar{K}$ scattering in P -wave and the ρ resonance from lattice QCD,” *Phys. Rev.* **D92**, 094502 (2015), arXiv:1507.02599 [hep-ph].
- [20] Raul A. Briceño, Jozef J. Dudek, Robert G. Edwards, and David J. Wilson, “Isoscalar $\pi\pi$ scattering and the σ meson resonance from QCD,” *Phys. Rev. Lett.* **118**, 022002 (2017), arXiv:1607.05900 [hep-ph].
- [21] Ruair Brett, John Bulava, Jacob Fallica, Andrew Hanlon, Ben Höz, and Colin Morningstar, “Determination of s - and p -wave $I = 1/2$ $K\pi$ scattering amplitudes in $N_f = 2 + 1$ lattice QCD,” *Nucl. Phys.* **B932**, 29–51 (2018), arXiv:1802.03100 [hep-lat].
- [22] Christian Walther Andersen, John Bulava, Ben Höz, and Colin Morningstar, “Elastic $I = 3/2$ p -wave nucleon-pion scattering amplitude and the $\Delta(1232)$ resonance from $N_f=2+1$ lattice QCD,” *Phys. Rev.* **D97**, 014506 (2018), arXiv:1710.01557 [hep-lat].
- [23] Dehua Guo, Andrei Alexandru, Raquel Molina, Maxim Mai, and Michael Döring, “Extraction of isoscalar $\pi\pi$ phase-shifts from lattice QCD,” *Phys. Rev.* **D98**, 014507 (2018), arXiv:1803.02897 [hep-lat].
- [24] Christian Andersen, John Bulava, Ben Höz, and Colin Morningstar, “The $I = 1$ pion-pion scattering amplitude and timelike pion form factor from $N_f = 2 + 1$ lattice QCD,” *Nucl. Phys.* **B939**, 145–173 (2019), arXiv:1808.05007 [hep-lat].
- [25] Jozef J. Dudek, Robert G. Edwards, Christopher E. Thomas, and David J. Wilson (Hadron Spectrum), “Resonances in coupled $\pi K - \eta K$ scattering from quantum chromodynamics,” *Phys. Rev. Lett.* **113**, 182001 (2014), arXiv:1406.4158 [hep-ph].
- [26] Jozef J. Dudek, Robert G. Edwards, and David J. Wilson (Hadron Spectrum), “An a_0 resonance in strongly coupled $\pi\eta, K\bar{K}$ scattering from lattice QCD,” *Phys. Rev.* **D93**, 094506 (2016), arXiv:1602.05122 [hep-ph].
- [27] Antoni Woss, Christopher E. Thomas, Jozef J. Dudek, Robert G. Edwards, and David J. Wilson, “Dynamically-coupled partial-waves in $\rho\pi$ isospin-2 scattering from lattice QCD,” *JHEP* **07**, 043 (2018), arXiv:1802.05580 [hep-lat].
- [28] Antoni J. Woss, Christopher E. Thomas, Jozef J. Dudek, Robert G. Edwards, and David J. Wilson, “The b_1 resonance in coupled $\pi\omega, \pi\phi$ scattering from lattice QCD,” (2019), arXiv:1904.04136 [hep-lat].
- [29] Christopher Helmes, Christian Jost, Bastian Knippschild, Bartosz Kostrzewa, Liuming Liu, Ferenc Pittler, Carsten Urbach, and Markus Werner (ETM), “Hadron-Hadron Interactions from $N_f = 2 + 1 + 1$ Lattice QCD: $I = 3/2$ πK Scattering Length,” *Phys. Rev.* **D98**, 114511 (2018), arXiv:1809.08886 [hep-lat].
- [30] L. Liu *et al.*, “Isospin-0 $\pi\pi$ s-wave scattering length from twisted mass lattice QCD,” *Phys. Rev.* **D96**, 054516 (2017), arXiv:1612.02061 [hep-lat].
- [31] Christopher Helmes, Christian Jost, Bastian Knippschild, Bartosz Kostrzewa, Liuming Liu, Carsten Urbach, and Markus Werner, “Hadron-Hadron Interactions from $N_f = 2 + 1 + 1$ lattice QCD: Isospin-1 $K\bar{K}$ scattering length,” *Phys. Rev.* **D96**, 034510 (2017), arXiv:1703.04737 [hep-lat].
- [32] Markus Werner *et al.*, “Hadron-Hadron Interactions from $N_f = 2 + 1 + 1$ Lattice QCD: The ρ -resonance,” *Eur. Phys. J. A* **56**, 61 (2020), arXiv:1907.01237 [hep-lat].
- [33] C. Culver, M. Mai, A. Alexandru, M. Döring, and F. X. Lee, “Pion scattering in the isospin $I=2$ channel from

- elongated lattices,” (2019), [arXiv:1905.10202 \[hep-lat\]](#).
- [34] Maxim Mai, Chris Culver, Andrei Alexandru, Michael Döring, and Frank X. Lee, “A cross-channel study of pion scattering from lattice QCD,” (2019), [arXiv:1908.01847 \[hep-lat\]](#).
- [35] M. Doring, U. G. Meißner, E. Oset, and A. Rusetsky, “Scalar mesons moving in a finite volume and the role of partial wave mixing,” *Eur. Phys. J. A* **48**, 114 (2012), [arXiv:1205.4838 \[hep-lat\]](#).
- [36] Matthias Fischer, Bartosz Kostrzewa, Maxim Mai, Marcus Petschlies, Ferenc Pittler, Martin Ueding, Carsten Urbach, and Markus Werner (ETM), “The ρ -resonance with physical pion mass from $N_f = 2$ lattice QCD,” (2020), [arXiv:2006.13805 \[hep-lat\]](#).
- [37] Antoni J. Woss, David J. Wilson, and Jozef J. Dudek (Hadron Spectrum), “Efficient solution of the multi-channel Lüscher determinant condition through eigenvalue decomposition,” *Phys. Rev. D* **101**, 114505 (2020), [arXiv:2001.08474 \[hep-lat\]](#).
- [38] John Bulava, Brendan Fahy, Ben Hörz, Keisuke J. Juge, Colin Morningstar, and Chik Him Wong, “ $I = 1$ and $I = 2$ $\pi - \pi$ scattering phase shifts from $N_f = 2 + 1$ lattice QCD,” *Nucl. Phys. B* **910**, 842–867 (2016), [arXiv:1604.05593 \[hep-lat\]](#).
- [39] Raul A. Briceño, Jozef J. Dudek, and Ross D. Young, “Scattering processes and resonances from lattice QCD,” *Rev. Mod. Phys.* **90**, 025001 (2018), [arXiv:1706.06223 \[hep-lat\]](#).
- [40] Maxwell T. Hansen and Stephen R. Sharpe, “Relativistic, model-independent, three-particle quantization condition,” *Phys. Rev. D* **90**, 116003 (2014), [arXiv:1408.5933 \[hep-lat\]](#).
- [41] Maxwell T. Hansen and Stephen R. Sharpe, “Expressing the three-particle finite-volume spectrum in terms of the three-to-three scattering amplitude,” *Phys. Rev. D* **92**, 114509 (2015), [arXiv:1504.04248 \[hep-lat\]](#).
- [42] Maxwell T. Hansen and Stephen R. Sharpe, “Perturbative results for two and three particle threshold energies in finite volume,” *Phys. Rev. D* **93**, 014506 (2016), [arXiv:1509.07929 \[hep-lat\]](#).
- [43] Maxwell T. Hansen and Stephen R. Sharpe, “Threshold expansion of the three-particle quantization condition,” *Phys. Rev. D* **93**, 096006 (2016), [Erratum: *Phys. Rev. D* **96**, 039901 (2017)], [arXiv:1602.00324 \[hep-lat\]](#).
- [44] Raúl A. Briceño, Maxwell T. Hansen, and Stephen R. Sharpe, “Relating the finite-volume spectrum and the two-and-three-particle S matrix for relativistic systems of identical scalar particles,” *Phys. Rev. D* **95**, 074510 (2017), [arXiv:1701.07465 \[hep-lat\]](#).
- [45] Raúl A. Briceño, Maxwell T. Hansen, and Stephen R. Sharpe, “Numerical study of the relativistic three-body quantization condition in the isotropic approximation,” *Phys. Rev. D* **98**, 014506 (2018), [arXiv:1803.04169 \[hep-lat\]](#).
- [46] Raúl A. Briceño, Maxwell T. Hansen, and Stephen R. Sharpe, “Three-particle systems with resonant subprocesses in a finite volume,” *Phys. Rev. D* **99**, 014516 (2019), [arXiv:1810.01429 \[hep-lat\]](#).
- [47] Tyler D. Blanton, Fernando Romero-López, and Stephen R. Sharpe, “Implementing the three-particle quantization condition including higher partial waves,” *JHEP* **03**, 106 (2019), [arXiv:1901.07095 \[hep-lat\]](#).
- [48] Fernando Romero-López, Stephen R. Sharpe, Tyler D. Blanton, Raúl A. Briceño, and Maxwell T. Hansen, “Numerical exploration of three relativistic particles in a finite volume including two-particle resonances and bound states,” *JHEP* **10**, 007 (2019), [arXiv:1908.02411 \[hep-lat\]](#).
- [49] Maxwell T. Hansen, Fernando Romero-López, and Stephen R. Sharpe, “Generalizing the relativistic quantization condition to include all three-pion isospin channels,” *JHEP* **20**, 047 (2020), [arXiv:2003.10974 \[hep-lat\]](#).
- [50] K. Polejaeva and A. Rusetsky, “Three particles in a finite volume,” *Eur. Phys. J. A* **48**, 67 (2012), [arXiv:1203.1241 \[hep-lat\]](#).
- [51] Ulf-G. Meißner, Guillermo Ríos, and Akaki Rusetsky, “Spectrum of three-body bound states in a finite volume,” *Phys. Rev. Lett.* **114**, 091602 (2015), [Erratum: *Phys. Rev. Lett.* **117**, no.6, 069902(2016)], [arXiv:1412.4969 \[hep-lat\]](#).
- [52] Hans-Werner Hammer, Jin-Yi Pang, and A. Rusetsky, “Three-particle quantization condition in a finite volume: 1. The role of the three-particle force,” *JHEP* **09**, 109 (2017), [arXiv:1706.07700 \[hep-lat\]](#).
- [53] H. W. Hammer, J. Y. Pang, and A. Rusetsky, “Three particle quantization condition in a finite volume: 2. general formalism and the analysis of data,” *JHEP* **10**, 115 (2017), [arXiv:1707.02176 \[hep-lat\]](#).
- [54] M. Döring, H. W. Hammer, M. Mai, J. Y. Pang, A. Rusetsky, and J. Wu, “Three-body spectrum in a finite volume: the role of cubic symmetry,” *Phys. Rev. D* **97**, 114508 (2018), [arXiv:1802.03362 \[hep-lat\]](#).
- [55] Jin-Yi Pang, Jia-Jun Wu, H. W. Hammer, Ulf-G. Meißner, and Akaki Rusetsky, “Energy shift of the three-particle system in a finite volume,” *Phys. Rev. D* **99**, 074513 (2019), [arXiv:1902.01111 \[hep-lat\]](#).
- [56] M. Mai and M. Döring, “Three-body unitarity in the Finite Volume,” *Eur. Phys. J. A* **53**, 240 (2017), [arXiv:1709.08222 \[hep-lat\]](#).
- [57] Maxim Mai and Michael Döring, “Finite-Volume Spectrum of $\pi^+\pi^+$ and $\pi^+\pi^+\pi^+$ Systems,” *Phys. Rev. Lett.* **122**, 062503 (2019), [arXiv:1807.04746 \[hep-lat\]](#).
- [58] P. Klos, S. König, H. W. Hammer, J. E. Lynn, and A. Schwenk, “Signatures of few-body resonances in finite volume,” *Phys. Rev. C* **98**, 034004 (2018), [arXiv:1805.02029 \[nucl-th\]](#).
- [59] Peng Guo and Vladimir Gasparian, “An solvable three-body model in finite volume,” *Phys. Lett. B* **774**, 441–445 (2017), [arXiv:1701.00438 \[hep-lat\]](#).
- [60] A. Jackura, C. Fernández-Ramírez, V. Mathieu, M. Mikhasenko, J. Nys, A. Pilloni, K. Saldaña, N. Sherrill, and A. P. Szczepaniak (JPAC), “Phenomenology of Relativistic $\mathbf{3} \rightarrow \mathbf{3}$ Reaction Amplitudes within the Isobar Approximation,” *Eur. Phys. J. C* **79**, 56 (2019), [arXiv:1809.10523 \[hep-ph\]](#).
- [61] Maxwell T. Hansen and Stephen R. Sharpe, “Lattice QCD and Three-particle Decays of Resonances,” (2019), [arXiv:1901.00483 \[hep-lat\]](#).
- [62] Ben Hörz and Andrew Hanlon, “Two- and three-pion finite-volume spectra at maximal isospin from lattice QCD,” *Phys. Rev. Lett.* **123**, 142002 (2019), [arXiv:1905.04277 \[hep-lat\]](#).
- [63] Chris Culver, Maxim Mai, Ruairí Brett, Andrei Alexandru, and Michael Döring, “Three body spectrum from lattice QCD,” *Phys. Rev. D* **101**, 114507 (2020), [arXiv:1911.09047 \[hep-lat\]](#).
- [64] M. Mai, M. Döring, C. Culver, and A. Alexandru, “Three-body unitarity versus finite-volume $\pi^+\pi^+\pi^+$

- spectrum from lattice QCD,” *Phys. Rev. D* **101**, 054510 (2020), [arXiv:1909.05749 \[hep-lat\]](#).
- [65] Tyler D. Blanton, Fernando Romero-López, and Stephen R. Sharpe, “ $I = 3$ Three-Pion Scattering Amplitude from Lattice QCD,” *Phys. Rev. Lett.* **124**, 032001 (2020), [arXiv:1909.02973 \[hep-lat\]](#).
- [66] Silas R. Beane, William Detmold, and Martin J. Savage, “n-Boson Energies at Finite Volume and Three-Boson Interactions,” *Phys. Rev.* **D76**, 074507 (2007), [arXiv:0707.1670 \[hep-lat\]](#).
- [67] William Detmold, Martin J. Savage, Aaron Torok, Silas R. Beane, Thomas C. Luu, Kostas Orginos, and Assumpta Parreno, “Multi-Pion States in Lattice QCD and the Charged-Pion Condensate,” *Phys. Rev.* **D78**, 014507 (2008), [arXiv:0803.2728 \[hep-lat\]](#).
- [68] Fernando Romero-López, Akaki Rusetsky, and Carsten Urbach, “Two- and three-body interactions in φ^4 theory from lattice simulations,” *Eur. Phys. J.* **C78**, 846 (2018), [arXiv:1806.02367 \[hep-lat\]](#).
- [69] S.R. Beane *et al.*, “Charged multi-hadron systems in lattice QCD+QED,” (2020), [arXiv:2003.12130 \[hep-lat\]](#).
- [70] Jozef J. Dudek, Robert G. Edwards, and Christopher E. Thomas, “S and D-wave phase shifts in isospin-2 pi pi scattering from lattice QCD,” *Phys. Rev.* **D86**, 034031 (2012), [arXiv:1203.6041 \[hep-ph\]](#).
- [71] J. Gasser and H. Leutwyler, “Light Quarks at Low Temperatures,” *Phys. Lett. B* **184**, 83–88 (1987).
- [72] J. Gasser and H. Leutwyler, “Thermodynamics of Chiral Symmetry,” *Phys. Lett. B* **188**, 477–481 (1987).
- [73] J. Gasser and H. Leutwyler, “Spontaneously Broken Symmetries: Effective Lagrangians at Finite Volume,” *Nucl. Phys. B* **307**, 763–778 (1988).
- [74] A. Abdel-Rehim *et al.* (ETM), “First physics results at the physical pion mass from $N_f = 2$ Wilson twisted mass fermions at maximal twist,” *Phys. Rev.* **D95**, 094515 (2017), [arXiv:1507.05068 \[hep-lat\]](#).
- [75] Y. Iwasaki, “Renormalization Group Analysis of Lattice Theories and Improved Lattice Action: Two-Dimensional Nonlinear O(N) Sigma Model,” *Nucl. Phys. B* **258**, 141–156 (1985).
- [76] Roberto Frezzotti, Pietro Antonio Grassi, Stefan Sint, and Peter Weisz (Alpha), “Lattice QCD with a chirally twisted mass term,” *JHEP* **08**, 058 (2001), [arXiv:hep-lat/0101001](#).
- [77] R. Frezzotti and G. C. Rossi, “Chirally improving Wilson fermions. I: O(a) improvement,” *JHEP* **08**, 007 (2004), [hep-lat/0306014](#).
- [78] Michael I. Buchoff, Jiunn-Wei Chen, and Andre Walker-Loud, “pi-pi Scattering in Twisted Mass Chiral Perturbation Theory,” *Phys. Rev. D* **79**, 074503 (2009), [arXiv:0810.2464 \[hep-lat\]](#).
- [79] Michael Peardon, John Bulava, Justin Foley, Colin Morningstar, Jozef Dudek, Robert G. Edwards, Balint Joo, Huey-Wen Lin, David G. Richards, and Keisuke Jimmy Juge (Hadron Spectrum), “A Novel quark-field creation operator construction for hadronic physics in lattice QCD,” *Phys. Rev. D* **80**, 054506 (2009), [arXiv:0905.2160 \[hep-lat\]](#).
- [80] Colin Morningstar, John Bulava, Justin Foley, Keisuke J. Juge, David Lenkner, Mike Peardon, and Chik Him Wong, “Improved stochastic estimation of quark propagation with Laplacian Heaviside smearing in lattice QCD,” *Phys. Rev. D* **83**, 114505 (2011), [arXiv:1104.3870 \[hep-lat\]](#).
- [81] Petros Dimopoulos *et al.*, “Topological susceptibility and η' meson mass from $N_f = 2$ lattice QCD at the physical point,” *Phys. Rev.* **D99**, 034511 (2019), [arXiv:1812.08787 \[hep-lat\]](#).
- [82] Christopher Michael and I. Teasdale, “Extracting Glueball Masses From Lattice QCD,” *Nucl. Phys.* **B215**, 433–446 (1983).
- [83] Benoit Blossier, Michele Della Morte, Georg von Hippel, Tereza Mendes, and Rainer Sommer, “On the generalized eigenvalue method for energies and matrix elements in lattice field theory,” *JHEP* **04**, 094 (2009), [arXiv:0902.1265 \[hep-lat\]](#).
- [84] Matthias Fischer, Bartosz Kostrzewa, Johann Ostermeyer, Konstantin Ottnad, Martin Ueding, and Carsten Urbach, “On the generalised eigenvalue method and its relation to Prony and generalised pencil of function methods,” (2020), [arXiv:2004.10472 \[hep-lat\]](#).
- [85] See Supplemental Material at [URL will be inserted by publisher].
- [86] Martin Ueding, “ $N_f = 2$ three pion $I = 3$ scattering data repository,” ().
- [87] R. Kaminski, J.R. Pelaez, and F.J. Yndurain, “The Pion-pion scattering amplitude. III. Improving the analysis with forward dispersion relations and Roy equations,” *Phys. Rev. D* **77**, 054015 (2008), [arXiv:0710.1150 \[hep-ph\]](#).
- [88] G. Colangelo, J. Gasser, and H. Leutwyler, “ $\pi\pi$ scattering,” *Nucl. Phys. B* **603**, 125–179 (2001), [arXiv:hep-ph/0103088](#).
- [89] Stephen L. Adler, “Consistency conditions on the strong interactions implied by a partially conserved axial-vector current,” *Phys. Rev.* **137**, B1022–B1033 (1965).
- [90] F.J. Yndurain, “Low-energy pion physics,” (2002), [arXiv:hep-ph/0212282](#).
- [91] J.R. Pelaez and F.J. Yndurain, “The Pion-pion scattering amplitude,” *Phys. Rev. D* **71**, 074016 (2005), [arXiv:hep-ph/0411334](#).
- [92] I. Caprini, G. Colangelo, and H. Leutwyler, “Regge analysis of the pi pi scattering amplitude,” *Eur. Phys. J. C* **72**, 1860 (2012), [arXiv:1111.7160 \[hep-ph\]](#).
- [93] T. Yamazaki *et al.* (CP-PACS), “ $I = 2$ pi pi scattering phase shift with two flavors of O(a) improved dynamical quarks,” *Phys. Rev. D* **70**, 074513 (2004), [arXiv:hep-lat/0402025](#).
- [94] Silas R. Beane, Paulo F. Bedaque, Kostas Orginos, and Martin J. Savage (NPLQCD), “ $I = 2$ pi-pi scattering from fully-dynamical mixed-action lattice QCD,” *Phys. Rev. D* **73**, 054503 (2006), [arXiv:hep-lat/0506013](#).
- [95] Silas R. Beane, Thomas C. Luu, Kostas Orginos, Assumpta Parreno, Martin J. Savage, Aaron Torok, and Andre Walker-Loud, “Precise Determination of the $I=2$ pi pi Scattering Length from Mixed-Action Lattice QCD,” *Phys. Rev. D* **77**, 014505 (2008), [arXiv:0706.3026 \[hep-lat\]](#).
- [96] S.R. Beane, E. Chang, W. Detmold, H.W. Lin, T.C. Luu, K. Orginos, A. Parreno, M.J. Savage, A. Torok, and A. Walker-Loud (NPLQCD), “The $I=2$ pipi S-wave Scattering Phase Shift from Lattice QCD,” *Phys. Rev. D* **85**, 034505 (2012), [arXiv:1107.5023 \[hep-lat\]](#).
- [97] Takuya Yagi, Shoji Hashimoto, Osamu Morimatsu, and Munehisa Ohtani, “ $I=2$ π - π scattering length with dynamical overlap fermion,” (2011), [arXiv:1108.2970 \[hep-lat\]](#).
- [98] Ziwen Fu, “Lattice QCD study of the s-wave $\pi\pi$ scat-

- tering lengths in the $I=0$ and 2 channels,” *Phys. Rev. D* **87**, 074501 (2013), arXiv:1303.0517 [hep-lat].
- [99] Kiyoshi Sasaki, Naruhito Ishizuka, Makoto Oka, and Takeshi Yamazaki (PACS-CS), “Scattering lengths for two pseudoscalar meson systems,” *Phys. Rev. D* **89**, 054502 (2014), arXiv:1311.7226 [hep-lat].
- [100] J. Bijnens, G. Colangelo, G. Ecker, J. Gasser, and M.E. Sainio, “Pion-pion scattering at low energy,” *Nucl. Phys. B* **508**, 263–310 (1997), [Erratum: *Nucl.Phys.B* 517, 639–639 (1998)], arXiv:hep-ph/9707291.
- [101] Jülich Supercomputing Centre, “JUQUEEN: IBM Blue Gene/Q Supercomputer System at the Jülich Supercomputing Centre,” *Journal of large-scale research facilities* **1** (2015), 10.17815/jlsrf-1-18.
- [102] Jülich Supercomputing Centre, “JURECA: Modular supercomputer at Jülich Supercomputing Centre,” *Journal of large-scale research facilities* **4** (2018), 10.17815/jlsrf-4-121-1.
- [103] Jülich Supercomputing Centre, “JUWELS: Modular Tier-0/1 Supercomputer at the Jülich Supercomputing Centre,” *Journal of large-scale research facilities* **5** (2019), 10.17815/jlsrf-5-171.
- [104] K. Jansen and C. Urbach, “tmLQCD: A Program suite to simulate Wilson Twisted mass Lattice QCD,” *Comput.Phys.Commun.* **180**, 2717–2738 (2009), arXiv:0905.3331 [hep-lat].
- [105] Abdou Abdel-Rehim, Florian Burger, Alber Deuzeman, Karl Jansen, Bartosz Kostrzewa, Luigi Scorzato, and Carsten Urbach, “Recent developments in the tmLQCD software suite,” *PoS LATTICE2013*, 414 (2014), arXiv:1311.5495 [hep-lat].
- [106] A. Deuzeman, K. Jansen, B. Kostrzewa, and C. Urbach, “Experiences with OpenMP in tmLQCD,” *PoS LATTICE2013*, 416 (2013), arXiv:1311.4521 [hep-lat].
- [107] Albert Deuzeman, Siebren Reker, and Carsten Urbach (ETM), “Lemon: an MPI parallel I/O library for data encapsulation using LIME,” *Comput. Phys. Commun.* **183**, 1321–1335 (2012), arXiv:1106.4177 [hep-lat].
- [108] M. A. Clark, R. Babich, K. Barros, R. C. Brower, and C. Rebbi, “Solving Lattice QCD systems of equations using mixed precision solvers on GPUs,” *Comput. Phys. Commun.* **181**, 1517–1528 (2010), arXiv:0911.3191 [hep-lat].
- [109] R. Babich, M. A. Clark, B. Joo, G. Shi, R. C. Brower, and S. Gottlieb, “Scaling Lattice QCD beyond 100 GPUs,” in *SC11 International Conference for High Performance Computing, Networking, Storage and Analysis Seattle, Washington, November 12-18, 2011* (2011) arXiv:1109.2935 [hep-lat].
- [110] M. A. Clark, Bálint Joó, Alexei Strelchenko, Michael Cheng, Arjun Gambhir, and Richard Brower, “Accelerating Lattice QCD Multigrid on GPUs Using Fine-Grained Parallelization,” (2016), arXiv:1612.07873 [hep-lat].
- [111] R Core Team, *R: A Language and Environment for Statistical Computing*, R Foundation for Statistical Computing, Vienna, Austria (2019).
- [112] Bartosz Kostrzewa, Johann Ostmeier, Martin Ueding, and Carsten Urbach, “hadron: package to extract hadronic quantities,” <https://github.com/HISKP-LQCD/hadron> (2020), R package version 3.0.1.
- [113] Martin Ueding, *paramvalf: Parameter Value Analysis Framework* (), r package version 2.7.0.
- [114] Ulli Wolff (ALPHA), “Monte Carlo errors with less errors,” *Comput. Phys. Commun.* **156**, 143–153 (2004), [Erratum: *Comput. Phys. Commun.*176,383(2007)], arXiv:hep-lat/0306017 [hep-lat].

Supplemental material for the Letter:
Scattering matrix elements of two and three physical pions at maximal isospin

EXTRACTION OF THE ENERGY LEVELS

In this section, we provide more details regarding the extraction of energy levels from the correlation functions of two and three pions. The required quark diagrams are shown in Figure S1. We compute the integrated autocorrelation time [114] of the correlators, and find in all cases that $\tau_{\text{int}} < 1$. Thus, we treat our correlation functions as decorrelated.

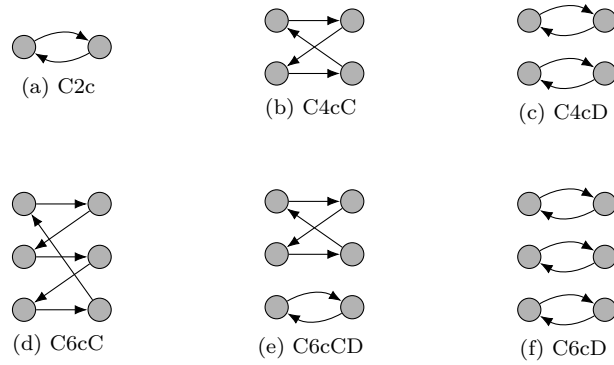


FIG. S1. Quark diagrams for two- and three- π^+ correlation functions.

Details on treatment of thermal pollutions

The spectral composition of the three-pion correlation function (with periodic boundary conditions) reads

$$\sum_m \sum_n \langle n | O_\Gamma(\mathbf{P}, \mathbf{q}_1, \mathbf{q}_2) | m \rangle \langle m | O_\Gamma^\dagger(\mathbf{P}, \mathbf{q}_3, \mathbf{q}_4) | n \rangle e^{-E_n \cdot (T-t)} e^{-E_m t}.$$

This means that there will be contributions from all possible states m and n with the correct quantum numbers. The desired signal arises when m is the vacuum, and the n is the desired three-pion state, or *vice versa*. Thermal states arise when m is an intermediate two-pion state and n a one-pion state. To illustrate this, let us assume that n is a one-pion state $|\mathbf{p}_1\rangle$ and m a two-pion state $|\mathbf{p}_2, \mathbf{p}_3\rangle$ with free energies given by the dispersion relation. Only summands where $\langle \mathbf{p}_1 | O_\Gamma | \mathbf{p}_2, \mathbf{p}_3 \rangle \neq 0$ contribute, i.e. the three-pion operator O_Γ must couple to the momenta \mathbf{p}_1 , \mathbf{p}_2 and \mathbf{p}_3 . The individual particle momenta that couple to a multi-particle operator can be inferred from group theory. Consider the frame $\mathbf{P}^2 = 0$, then the three-pion operator will be in some irrep Γ^- , and the single pion always in the A_1^- . Therefore, the two-pion system needs to be in the opposite parity irrep Γ^+ such that $A_1^- \otimes \Gamma^+ = \Gamma^-$. Note that only the irreps for $\mathbf{P}^2 = 0$ have a parity index, that is, in moving frames parity is not a good quantum number. In this situation, the momenta of the two-pion system can only take the values that actually couple into the irrep of the three-particle operator.

The allowed contributions are generated from all permutations of the three-pion individual momenta using the prescription described above. Using the measured pion mass M_π and the free particle dispersion relation (assuming weak interactions between the two pions) we compute the energy $E_\pi(\mathbf{p}_1)$ and $E_{2\pi}(\mathbf{p}_2, \mathbf{p}_3)$. The time dependence is given by $\exp(-(E_{2\pi} - E_\pi)t)$ in the forward term. We introduce $\Delta E := E_{2\pi} - E_\pi$ and write this as $\exp(-\Delta E t)$. There is an additional backward propagating part as well which goes as $\exp(-\Delta E \cdot (T - t))$. Together they either form a cosh (sum) or a sinh (difference). For three pions we only have time-even operators and therefore everything will have a cosh-shape. We can regroup the exponentials into an overall amplitude $\exp(-(E_{2\pi} + E_\pi)T)$ and a time

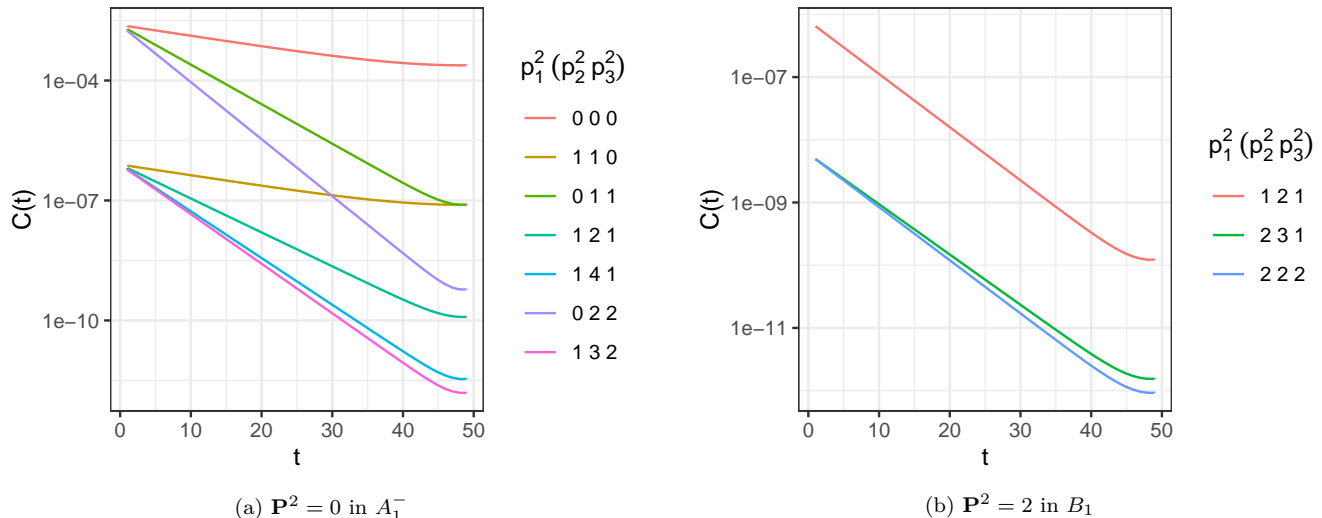


FIG. S2. Possible thermal contributions to the three-pion correlator matrix in the cA2.09.48 ensemble. Each line corresponds to a particular combination of the individual particle momentum magnitudes of the one-pion (\mathbf{p}_1) and the two-pion system (\mathbf{p}_2 and \mathbf{p}_3).

dependent factor $\exp(-(E_{2\pi} - E_\pi)t)$. We can already see that low energies lead to higher amplitudes whereas low energy differences lead to a weak time dependence. The largest contributions therefore have rather small momenta.

Figure S2 shows the contributing thermal states for two cases, left the A_1^- irrep in the $\mathbf{P}^2 = 0$ frame, right the B_1 irrep in the $\mathbf{P}^2 = 2$ frame. Here the largest contribution is coming from ($\mathbf{p}_1^2 = 0, \mathbf{p}_2^2 = 0, \mathbf{p}_3^2 = 0$) and ($\mathbf{p}_1^2 = 1, \mathbf{p}_2^2 = 2, \mathbf{p}_3^2 = 1$), respectively. The other possible contributions are suppressed by two orders of magnitude or even exponentially.

Our thermal state treatments can only treat a single thermal state, therefore we need to find the dominating one. We tally the time dependence of the various thermal states (assuming matrix elements are of equal size). Taking the largest contribution at $t = 10$ as a reference, we then have an energy estimate for the strongest thermal pollution in the correlator matrix.

To illustrate this procedure, we will look at $\mathbf{P}^2 = 2$ with $\Gamma = B_1$. The three-particle momenta that couple to the operator below our threshold are listed in Table S1. As the three particles are indistinguishable, we can partition them at will into a one-pion and two-pion state. The two-particle momenta must again be a valid two-particle system, otherwise they cannot be an intermediate thermal state. Table S2 lists the two-particle contributions in the B_1 irrep.

\mathbf{P}^2	Irrep	\mathbf{p}_1	\mathbf{p}_2	\mathbf{p}_3
2	B_1	(0, 1, -1)	(0, 0, 1)	(1, 0, 0)
2	B_1	(1, 1, 0)	(1, 0, 0)	(-1, 0, 0)
2	B_1	(-1, 1, 0)	(1, 0, 0)	(1, 0, 0)

TABLE S1. Selection of three-pion individual momenta couplings.

\mathbf{P}^2	Irrep	\mathbf{p}_2	\mathbf{p}_3
1	B_1	(-1, 0, 1)	(1, 0, 0)
2	B_1	(1, 1, -1)	(0, 0, 1)
4	B_1	(0, -1, 1)	(0, 1, 1)

TABLE S2. Selection of two-pion individual momenta couplings.

The following list contains a couple of momentum choices that are checked by the algorithm.

- We take (0, 1, -1) for the one pion and (0, 0, 1) and (1, 0, 0) for the other two. The two-pion system has $\mathbf{P}^2 = 2$, but the lowest contribution *in that irrep* has larger momenta. So this does not contribute.
- The single pion has $\mathbf{p}_1 = (1, 1, 0)$ and the two-pion system gets $\mathbf{p}_2 = (1, 0, 0)$ and $\mathbf{p}_3 = (-1, 0, 0)$. The two-

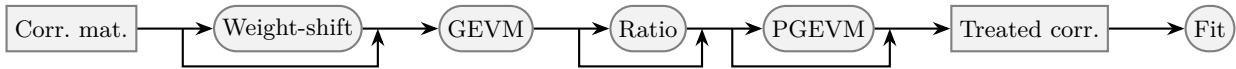


FIG. S3. Treatment of correlator matrices before fitting.

pion system therefore has total momentum $\mathbf{P}^2 = 0$, but there is no contribution to B_1 in that moving frame. Therefore this example does not contribute to the thermal states.

- A contribution is obtained using $(1, 0, 0)$ for the one pion, and $(0, 1, -1)$ and $(0, 0, 1)$ for the two-pion system. In the latter, we have $\mathbf{P}^2 = 1$, which corresponds to the first entry in Table S2 (albeit after an inconsequential global rotation). This contributes as a thermal state, incidentally it is the largest one as shown in Figure S2b.

Using this method we determine the leading thermal state for every correlator matrix and can use this as input for thermal state treatments, detailed below.

General technicalities

Multi-particle correlators in general are contaminated with excited states at early times, and with thermal pollution at late time slices. Fitting too early will overestimate the energy, while fitting too late may underestimate it. In order to obtain a robust energy estimate, we use combinations of different methods to attenuate these issues.

The order of application of these methods is illustrated with a flow chart in Figure S3. We will explain them in order. First the correlator matrices can optionally be treated with weight-shift-reweight [70] to suppress thermal states at the cost of larger statistical uncertainty. Then we independently use the original and treated correlator matrix and apply the GEVM, which yields the principal correlators. These principal correlators can be used to build ratios [17, 31] or left as-is. All variants can optionally be fed into the Prony Generalized Eigenvalue Method (PGEVM) [84] with $t_0 = 2$ fixed to suppress excited states. The PGEVM with δ_0 fixed did not produce credible results.

The resulting treated correlators are evaluated by looking at the so called effective mass. The simplest definition of it is the “log effective mass”

$$m_{\text{eff}}(t) = -\log \frac{C(t)}{C(t+1)}, \quad (\text{S1})$$

which assumes a signal proportional to $\exp(-Et)$ only. There are generalizations that take back-propagation, shifting or weighting into account. Depending on the treatment of the correlator we choose the appropriate effective mass. Not all of the 8 treatment combination are sensible to take. We will present the ones that yield sensible results.

No treatment: When no thermal states contribute (like in E irreps), a simple cosh-like model is fitted:

$$C(t) = A_0 [\exp(-E_0 t) + \exp(-E_0 \cdot (T - t))] . \quad (\text{S2})$$

If thermal states are present in the given irrep, a two-state model with constrained second energy E_1 will be used.

$$C(t) = A_0 [\exp(-E_0 t) + \exp(-E_0 \cdot (T - t))] + A_1 [\exp(-E_1 t) + \exp(-E_1 \cdot (T - t))] . \quad (\text{S3})$$

The constraint is implemented by an additional term in the χ^2 function to be minimized, namely a simple normally distributed prior,

$$\exp\left(-\frac{(E_1 - \bar{E}_1)^2}{(\Delta E_1)^2}\right), \quad (\text{S4})$$

where E_1 is the fit parameter, \bar{E}_1 is the determined central value for the thermal energy and ΔE_1 the uncertainty stemming from using the measured pion mass in the dispersion relation.

PGEVM: This method works well when there are no significant thermal state contributions. We fit a simple exponential model to the early time slices.

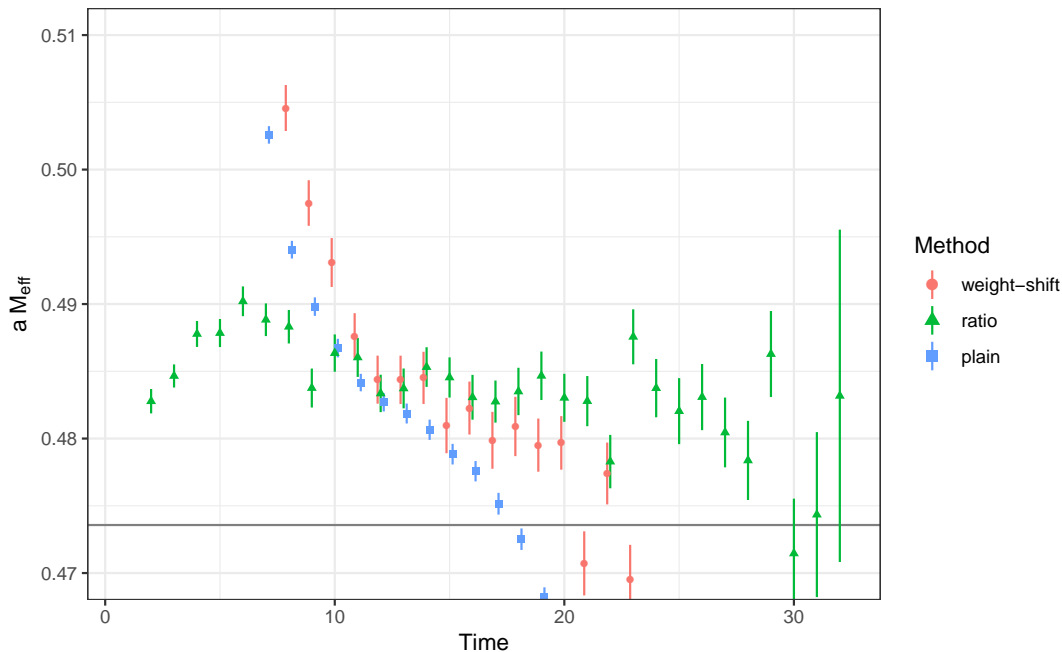


FIG. S4. Effective mass for the three pion ground state on the cA2.60.32 ensemble. Shown are in blue the plain correlator without any thermal state treatment, in red the correlator treated with weight-shift-reweight and in green the ratio R_3 shifted upwards by $3M_\pi$. The solid line marks the non-interacting energy.

Ratio: We take the ratio of the principal correlator (no weight-shift applied) and form ratios with the one-pion correlation function:

$$R_2(t) = \frac{C_{2\pi}(t) - C_{2\pi}(t+1)}{C_\pi(t)^2 - C_\pi(t+1)^2} \quad (\text{S5})$$

$$R_3(t) = \frac{C_{3\pi}(t)/C_\pi(t) - C_{3\pi}(t+1)/C_\pi(t+1)}{C_\pi(t)^2 - C_\pi(t+1)^2}. \quad (\text{S6})$$

The ratio R_3 is chosen as a double ratio such that in the numerator, thermal state contributions from single pions are removed. The resulting sinh-like correlator needs to be divided by another sinh-like expression to yield a cosh-like ratio. Among different ratio expressions tested, this is the most fruitful one. An exponential model is fitted to the ratios where the signal behaves like $R_2(t) \sim \exp(-(E_{2\pi} - 2E_\pi)t)$ and $R_3(t) \sim \exp(-(E_{3\pi} - 3E_\pi)t)$. This is only valid for small time slices, as backwards propagating parts are not included in this method.

Figure S4 shows a comparison between no treatment, weight-shift-reweight and the ratio R_3 for a case with heavy thermal pollution. One can see how the plain correlator does not show any plateau due to the high pollution. The weighted correlator has a plateau between $t_1 = 12$ and $t_2 = 14$, but still shows a drop. This likely stems from the second leading thermal state as visible in Figure S2a. The ratio however has a long plateau that is compatible with the weight-shift-reweight method. In general we see that with the ratio method it is possible to fit energy levels with strong thermal pollution when other methods fail to produce a plateau. The statistical uncertainty from the energy determination with the ratio is also lower than with other methods in most cases.

Weight-shift: The correlator matrix has the leading thermal state removed and therefore the principal correlators can be fitted with a cosh-like model which incorporates the weight-shift-reweight procedure.

Weight-shift and PGEVM: In general the additional suppression of excited states by the application of the PGEVM works well after weight-shift has been applied beforehand. The resulting correlator is fitted with an exponential model. Fit ranges can be chosen early enough such that the neglect of backwards propagating parts is not significant.

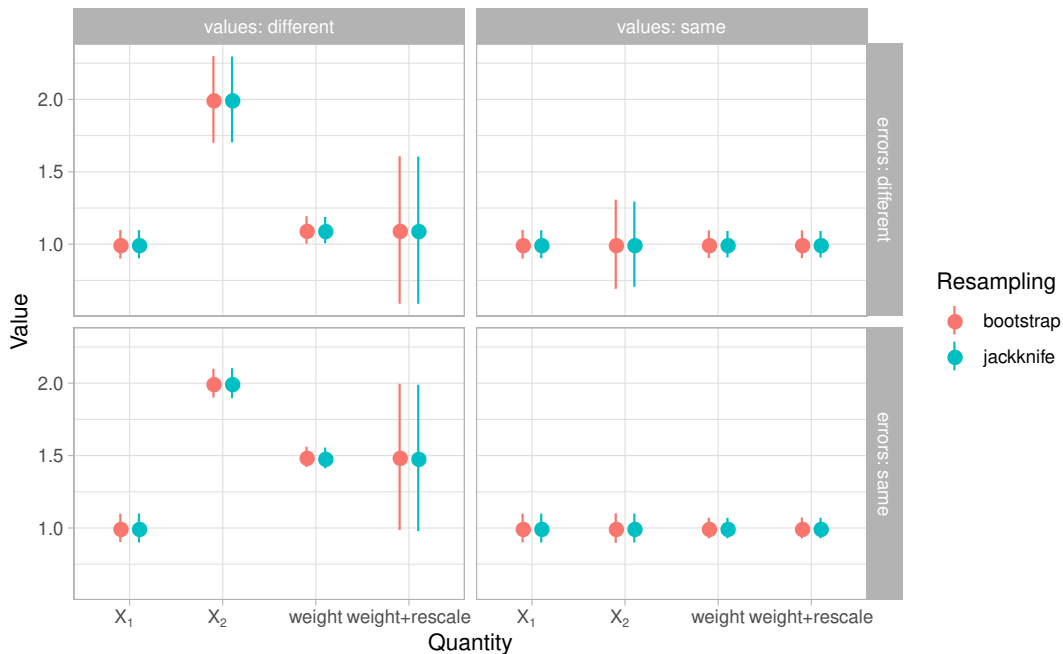


FIG. S5. Combination of fit results from two different methods to a weighted average and finally the rescaled distribution. Columns show different and same central values, rows show different and same statistical errors in the two measurements.

In some cases the thermal states are so pronounced that no plateau can be identified, even after applying the PGEVM. In these cases the method is not used for that particular level. These cases work much better with either the multi-state model, weight-shift-reweight or the combination of weight-shift-reweight and the PGEVM. The ratio method seems to be the most robust one, it shows plateaus even when other methods fail to produce one. Also, the statistical uncertainty seems to be lower compared to the other methods in general.

The principal correlators are inherently correlated in the time direction as one observes that the jitter between adjacent time slices is lower than suggested by the statistical uncertainty. We therefore use a correlated χ^2 expression in the fit in order to treat this correlation sensibly.

Details on combining methods and fit range choices

For every principal correlator we attempt to extract the energy with all our methods. If a plateau can be identified, we use the extracted energy level. All such determinations per principal correlator are combined with a weighted average. In order to incorporate the systematic spread between the central values, we also compute a systematic error scaling factor as introduced in Ref. [32]. By scaling the resampling distribution of the weighted average, we obtain a distribution that reflects both the statistical and the systematic uncertainties.

To illustrate this method, one can generate a numerical example with two distributions X_1 and X_2 generated in four ways, where either the central values and/or widths can be chosen to be the same or different. All combinations thus give four cases, which are shown in the quadrants of Figure S5. The distributions X_1 and X_2 are shown as the first two pairs of points in each quadrant. Then the third pair shows the pairwise weighted average of the two distributions. And the fourth pair shows the resulting distribution after the rescaling. One can nicely see how the weighted average gravitates toward the distribution with a lower width (hence higher weight) and how the rescaling incorporates the spread between the central values. The method works well for bootstrap and jackknife resampling.

In order to choose appropriate fit ranges for the different methods, we proceed iteratively, selecting fit ranges by eye (taking into account several metrics beyond just the effective mass). Some energy levels show significant tension between the different fitting methods after this first iteration. In these cases, we re-evaluate the plateaus to arrive at our final choices.

FITTING THE SPECTRUM

Here, we aim to extend the discussion of the fitting procedure of the spectrum to the quantization condition. The a summary of the frames, irreps and energies used in this work is shown in Table S3.

\mathbf{P}^2	Irrep	E/M_π range	\mathbf{P}^2	Irrep	E/M_π range
0	A1g	[2.03, 4.85]	0	A1u	[3.09, 6.05]
0	Eg	[4.71, 6.31]	0	Eu	[5.91, 5.92]
1	A1	[2.63, 6.64]	1	A2	[3.92, 3.92]
2	A1	[2.95, 5.79]	2	A2	[4.37, 4.99]
3	A1	[3.14, 4.29]	3	A2	[4.69, 6.40]
3	E	[4.00, 4.00]	3	E	[5.70, 8.06]
4	A1	[2.05, 4.79]	4	A2	[3.92, 6.42]
4	B1	[4.86, 4.86]	4	B2	[6.42, 6.42]

(a) cA2.09.48, two pions (b) cA2.09.48, three pions

\mathbf{P}^2	Irrep	E/M_π range	\mathbf{P}^2	Irrep	E/M_π range
0	A1g	[2.01, 3.99]	0	A1g	[2.02, 4.20]
0	Eg	[3.09, 3.88]	0	Eg	[3.21, 4.08]
1	A1	[2.29, 4.15]	1	A1	[2.32, 4.38]
1	B1	[3.28, 3.28]	1	B1	[3.43, 3.43]
1	B2	[4.09, 4.09]	1	B2	[4.25, 4.26]
1	E	[3.31, 4.02]	1	E	[3.41, 4.26]
2	A1	[2.46, 4.26]	2	A1	[2.50, 4.44]
2	A2	[3.50, 3.50]	2	A2	[3.67, 3.67]
2	B1	[3.45, 3.45]	2	B1	[3.60, 3.60]
2	B2	[4.22, 4.22]	2	B2	[4.39, 4.39]
3	A1	[2.59, 4.46]	3	A1	[2.65, 4.66]
3	E	[2.84, 4.44]	3	E	[2.94, 4.68]
4	A1	[2.03, 3.13]	4	A1	[2.02, 3.28]
4	B1	[3.12, 3.12]	4	B1	[3.21, 3.21]

(c) cA2.30.48, two pions (d) cA2.30.48, three pions (e) cA2.60.32, two pions (f) cA2.60.32, three pions

TABLE S3. Summary of energy levels included in this work.

General technicalities

In both, the two and three-particle sector, we define the χ^2 as:

$$\chi^2 = \sum_{ij} (E_i^{\text{data}} - E_i^{\text{predicted}}) (C)_{ij}^{-1} (E_i^{\text{data}} - E_j^{\text{predicted}}), \quad (\text{S7})$$

where C is the covariance matrix of the energy levels, estimated from the bootstrap samples. Best fit parameters are obtained using the Levenberg-Marquardt algorithm.

The range of validity of the quantization conditions is limited by the first inelastic threshold. This is $E^* = 4M_\pi$ ($5M_\pi$) for the two-particle (three-particle) quantization condition. We generally include levels up to that threshold, however, for the physical point ensemble (cA2.09.48), we have included levels higher up in energy. Since the $2\pi \rightarrow 4\pi$, and $3\pi \rightarrow 5\pi$ couplings are very small, we expect this to be a valid approximation. In fact, phenomenological studies set the first relevant inelasticity to be the $\rho\pi$ channel ($E^* \sim 7M_\pi$ for physical kinematics) [87, 90, 91].

Another issue to be discussed is the relevance of exponentially-suppressed effects that affect the energy levels and the quantization conditions. We expect them to be very small for the heaviest ensembles, where $M_\pi L > 5$. For the ensemble at the physical point (cA2.09.48), we however have $M_\pi L \sim 3$, which means $e^{-M_\pi L} \sim 5\%$. Given the statistical uncertainties of our results for that ensemble, we still expect that our error is dominated by the statistical one.

Additional discussion on two-pion fits

One interesting point to discuss is the suitability of the δ_0 parametrization. It has been customary to use a standard effective range expansion parametrization (ERE) for $I = 2$ $\pi\pi$ scattering:

$$\frac{k}{M_\pi} \cot \delta_0 = -\frac{1}{M_\pi a_0} + \frac{1}{2} M_\pi r \left(\frac{k}{M_\pi} \right)^2 + M_\pi^3 P \left(\frac{k}{M_\pi} \right)^4. \quad (\text{S8})$$

However, the presence of the Adler zero limits the radius of convergence to $k^2 \sim 0.5M_\pi^2$. For this reason, explicitly incorporating the Adler zero must improve the radius of convergence, and has been shown to describe the data better [65]. Here we compare again the two fit modes. The ERE results are shown in Table S4. As can be seen, the values of χ^2 in the case of the ERE fits are always larger than their Adler-zero counterparts—Table II. This further supports the usage of the Adler-zero parametrization for $I = 2$ $\pi\pi$ scattering.

Ensemble	$M_\pi a_0$	$M_\pi r$	$M_\pi^3 P$	χ^2/dof
cA2.60.32	0.2198(55)	1.1(2)	—	28.12/(16-2)
cA2.60.32	0.2177(56)	2.1(5)	-0.16(8)	24.26/(16-3)
cA2.30.48	0.194(20)	1.4(5)	—	20.22/(16-2)
cA2.09.48	0.064(11)	3.9(1.1)	—	14.00/(10-2)

TABLE S4. Two-particle fits to the standard effective range expansion (ERE) model in Eq. S8.

We also include the phase shift plots in the heavier ensembles: Figure S6 for cA2.30.48, and Figure S7 for cA2.60.32. In the case of the s -wave phase shift, we also compare to LO ChPT. As can be seen, the ChPT prediction describes the data at heavier pion masses—compare to Figure 2.

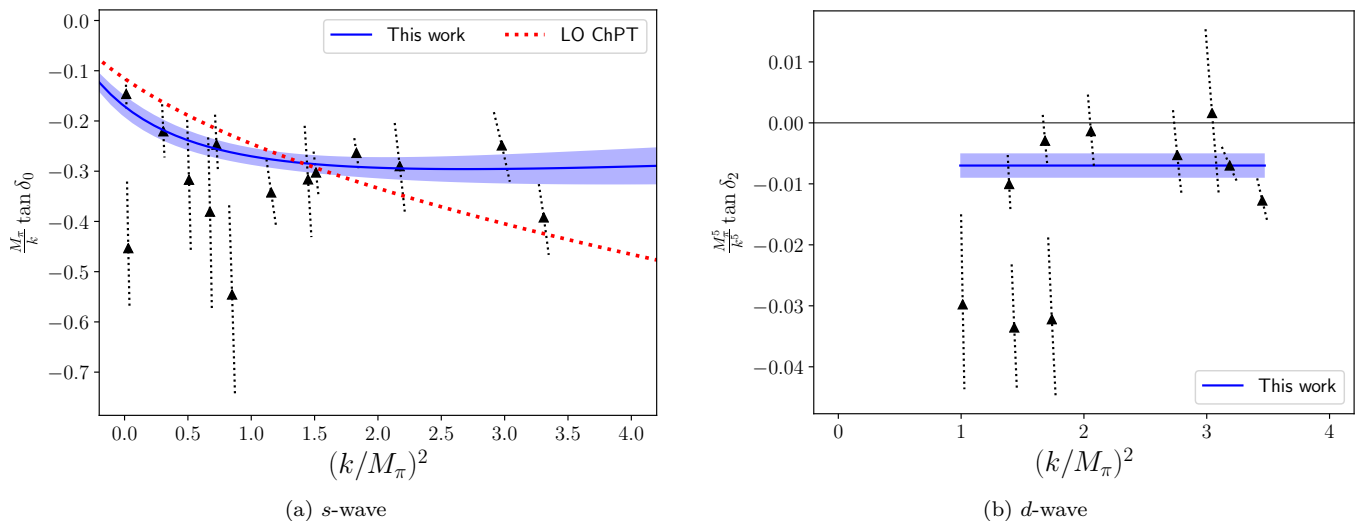


FIG. S6. s - and d -wave phase shift for the ensemble cA2.30.48. For s -wave we use a model that incorporates the Adler-zero, whereas for d -wave we fit to a constant in the region for which we have data. Two points have been omitted in the plot due to the very large errorbars.

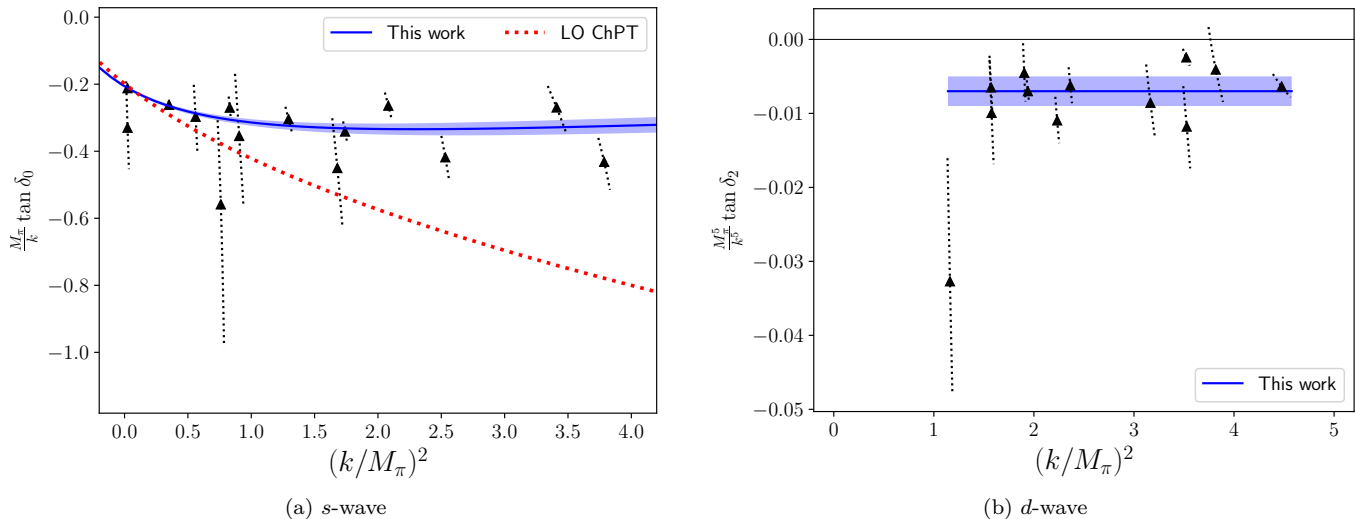


FIG. S7. s - and d -wave phase shift for the ensemble cA2.60.32. For s -wave we use a model that incorporates the Adler-zero, whereas for d -wave we fit to a constant in the region for which we have data. Two points have been omitted in the plot due to the very large errorbars.

Additional discussion on three-pion fits

First, we perform a global fit to two- and three-particle levels that includes only a constant term only in $\mathcal{K}_{3,\text{df}}$. This is shown in Table S5. As can be seen, the quality of the fit is significantly worse for the heavier ensembles than in the linear fits of Table IV. For the ensemble at the physical point (cA2.09.48), the value of χ^2 is basically the same, but in both cases $\mathcal{K}_{3,\text{df}}$ is compatible with zero. We thus conclude that the linear model of $\mathcal{K}_{3,\text{df}}$ in Eq. 6 is more appropriate for this system.

	$1/B_0$	B_1	$M_\pi^2 \mathcal{K}_{\text{df},3}^{\text{iso},0}$	$M_\pi^2 \mathcal{K}_{\text{df},3}^{\text{iso},1}$	χ^2/dof
cA2.60.32	-0.2050(49)	-1.7(2)	900(1000)	—	71.08/(43-3)
cA2.30.48	-0.154(20)	-1.5(5)	-4000(1700)	—	44.43/(33-3)
cA2.09.48	-0.0482(86)	-1.3(1.1)	-200(600)	—	19.24/(19-3)

TABLE S5. Two- and three-pion fits using the Adler-zero form ($z^2 = M_\pi^2$, fixed). Here we assume that $\mathcal{K}_{3,\text{df}}$ is given by a constant: $\mathcal{K}_{3,\text{df}} = \mathcal{K}_{\text{df},3}^{\text{iso},0}$.

Next, the full covariance matrices of the fits in Eq. IV are provided. We use the form $C = DRD$, with D being a

diagonal matrix with the standard errors of the parameters. We ordered the entries as: $(B_0, B_1, M_\pi^2 \mathcal{K}_{\text{df},3}^{\text{iso},0}, M_\pi^2 \mathcal{K}_{\text{df},3}^{\text{iso},1})$.

$$\begin{aligned} \text{cA2.09.48: } D &= \text{diag} (0.0086, 1.1, 800, 500), \\ R &= \begin{pmatrix} 1. & 0.73 & -0.37 & -0.02 \\ 0.73 & 1. & -0.25 & 0.11 \\ -0.37 & -0.25 & 1. & -0.71 \\ -0.02 & 0.11 & -0.71 & 1. \end{pmatrix}, \end{aligned} \tag{S9}$$

$$\begin{aligned} \text{cA2.30.48: } D &= \text{diag} (0.022, 0.5, 5600, 5000), \\ R &= \begin{pmatrix} 1.0 & 0.76 & -0.41 & 0.37 \\ 0.76 & 1.0 & -0.32 & 0.34 \\ -0.41 & -0.32 & 1.0 & -0.98 \\ 0.37 & 0.34 & -0.98 & 1.0 \end{pmatrix}, \end{aligned} \tag{S10}$$

$$\begin{aligned} \text{cA2.60.32: } D &= \text{diag} (0.0049, 0.2, 1500, 1800), \\ R &= \begin{pmatrix} 1.0 & 0.36 & -0.02 & 0.05 \\ 0.36 & 1.0 & 0.10 & 0.22 \\ -0.02 & 0.10 & 1.0 & -0.78 \\ 0.05 & 0.22 & -0.78 & 1.0 \end{pmatrix}, \end{aligned} \tag{S11}$$

We observe a large correlation within the two and three-particle sectors— the pairs B_0, B_1 , and $M_\pi^2 \mathcal{K}_{\text{df},3}^{\text{iso},0}, M_\pi^2 \mathcal{K}_{\text{df},3}^{\text{iso},1}$ are highly correlated. In contrast, the correlation between the two- and three-particle sector is milder.

Two- and three-pion spectrum

We conclude the discussion by comparing the spectrum from the lattice to the one predicted by the quantization conditions using the best fits. This is shown in Figure S8 for the ensemble at the physical point.

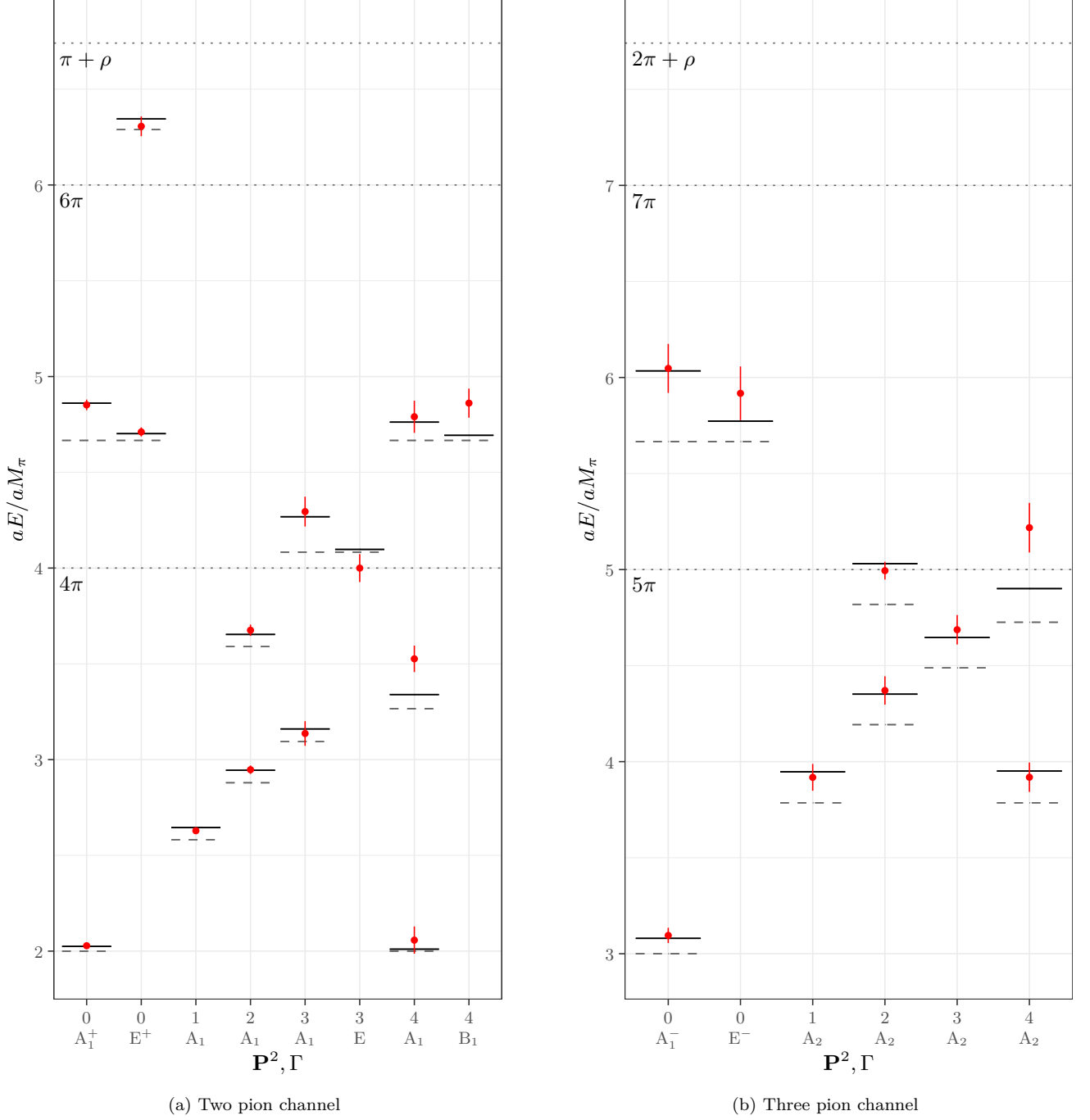


FIG. S8. The center-of-mass spectrum for two and three pions on the physical point ensemble (cA2.09.48). The red data points are the energy levels determined from the correlator. The black lines denote the prediction from the quantization condition. For the two-pion A_1 levels, and all three-pion levels, we use the fit in Table IV. For the non- A_1 two-pion levels, which are dominated by d -wave interactions, we use the fit in Table III. The short dashed gray lines denote the non-interacting energy levels. We also include the relevant inelastic thresholds as long dotted gray lines.